

Nuclear medium effects in Drell-Yan process

H. Haider,¹ M. Sajjad Athar,^{1,*} S. K. Singh,¹ and I. Ruiz Simo²

¹*Department of Physics, Aligarh Muslim University, Aligarh - 202 002, India*

²*Departamento de Física Atómica, Molecular y Nuclear,*

and Instituto de Física Teórica y Computacional Carlos I, Universidad de Granada, Granada 18071, Spain

We study the nuclear medium effects in Drell-Yan process using quark parton distribution functions calculated in a microscopic nuclear model which takes into account the effects of Fermi motion, nuclear binding and nucleon correlations through a relativistic nucleon spectral function. The contributions of π and ρ mesons as well as shadowing effects are also included. The beam energy loss is calculated using a phenomenological approach. The present theoretical results are compared with the experimental results of E772 and E886 experiments. These results are applicable to the forthcoming experimental analysis of E906 Sea Quest experiment at Fermi Lab.

PACS numbers: 13.40.-f, 21.65.-f, 24.85.+p, 25.40.-h

I. INTRODUCTION

Drell-Yan(DY) production of lepton pairs [1] from nucleons and nuclear targets is an important tool to study the quark structure of nucleons and its modification in the nuclear medium. In particular, the proton induced DY production of muon pairs on nucleons and nuclei provides a direct probe to investigate the quark parton distribution functions(PDFs). In a DY process(shown in Fig.1), a quark of beam(target) hadron gets annihilated from the antiquark of target(beam) hadron and gives rise to a photon which in turn gives lepton pairs of opposite charge. The basic process is $q^{b(t)} + \bar{q}^{t(b)} \rightarrow l^+ + l^-$, where b and t indicate the beam proton and the target nucleon/hadron. A quark(antiquark) in the beam carrying a longitudinal momentum fraction x_b interacts with an antiquark(quark) in the target carrying longitudinal momentum fraction x_t of the target momentum per nucleon to produce a virtual photon. The cross section per target nucleon $\frac{d^2\sigma}{dx_b dx_t}$ in the leading order is given by [2]:

$$\frac{d^2\sigma}{dx_b dx_t} = \frac{4\pi\alpha^2}{9Q^2} \sum_f e_f^2 \{ q_f^b(x_b, Q^2) \bar{q}_f^t(x_t, Q^2) + \bar{q}_f^b(x_b, Q^2) q_f^t(x_t, Q^2) \} \quad (1)$$

where α is the fine structure constant, e_f is the charge of quark/antiquark of flavor f, Q^2 is the photon virtuality and $q_f^{b(t)}(x)$ and $\bar{q}_f^{t(b)}(x)$ are the beam(target) quark/antiquark PDFs of flavour f.

This process is directly sensitive to the antiquark parton distribution functions $\bar{q}(x)$ in target nuclei which has also been studied by DIS experiments through the observation of EMC effect. Quantitatively the EMC effect describes the nuclear modification of nucleon structure function $F_2(x_t)$ for the bound nucleon defined as

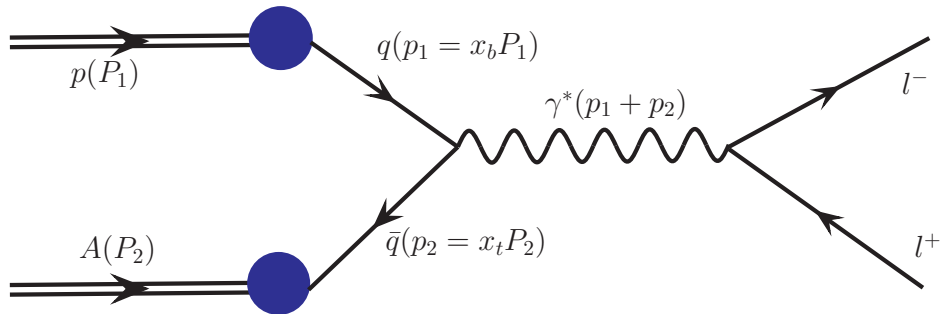


FIG. 1: Drell-Yan process: Here p stands for a proton and A for a proton or a nucleus. In the brackets four momenta of the particles are mentioned.

*Electronic address: sajathar@gmail.com

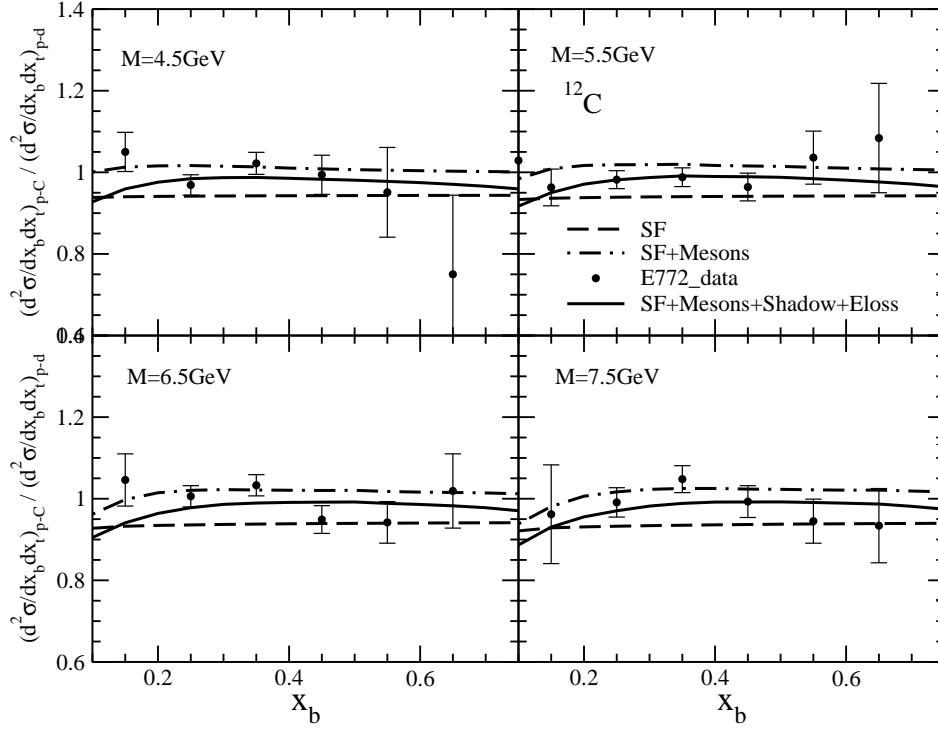


FIG. 2: $\frac{(\frac{d\sigma}{dx_b dx_t})_{p-d}}{(\frac{d\sigma}{dx_b dx_t})_{p-d}^{12C}}$ vs x_b at $E=800\text{GeV}(\sqrt{s_N}=38.8\text{GeV})$. Spectral function: dashed line, including mesonic contribution: dashed-dotted line and the results obtained using the full model i.e. spectral function+meson cloud contributions+shadowing effects+energy loss: solid line. The results in the different columns are obtained at different values of $M(=\sqrt{Q^2})$. Experimental points are data of E772 experiment [37, 49].

$F_2(x_t) = x_t \sum_f e_f^2 [q_f(x_t) + \bar{q}_f(x_t)]$ and gives information about the modification of the sum of quark and anti-quark PDFs [3, 4] which is dominated by the valence quarks in the high x_t region ($x_t > 0.3$). In the low x_t region ($x_t \leq 0.3$), where sea quarks are expected to give dominant contribution, the study of $F_2(x_t)$ gives information about sea quark and antiquark PDFs. Thus, nuclear modifications are phenomenologically incorporated in $q(x_t)$ and $\bar{q}(x_t)$ using the experimental data on $F_2(x_t)$ and are used to analyze the DY yields from nuclear targets. Some authors succeed in giving a satisfactory description of DIS and DY data on nuclear targets using same set of nuclear $q(x)$ and $\bar{q}(x)$ [5], while some others find it difficult to provide a consistent description of DIS and DY data using the same set of nuclear PDFs [6]. On the other hand, there are many theoretical attempts to describe the nuclear modifications of quark and antiquark PDFs to explain DIS which have also been used to understand the DY process on nuclear targets [7]-[23]. The known nuclear modifications discussed in literature in the case of DIS are (a) modification of nucleon structure inside the nuclear medium, (b) a significantly enhanced contribution of subnucleonic degrees of freedom like pions or quark clusters in nuclei and (c) nuclear shadowing. However, in the case of DY processes there is an additional nuclear effect due to initial state interaction of beam partons with the target partons which may be present before the hard collisions of these partons giving rise to lepton pairs. As the initial beam traverses the nuclear medium it loses energy due to interaction of beam partons with nuclear constituents of the target. This can be visualized in terms of the interaction of hadrons or its constituents with the constituents of the target nucleus through various inelastic processes leading to energy loss of the interacting beam partons. This has been studied phenomenologically using available parameterization of nuclear PDFs or theoretically in models based on QCD or Glauber approaches taking into account the effect of shadowing which also plays an important role in the low x_t region, however, any consensus in the understanding of physics behind the beam energy loss has been lacking. In this scenario most of the calculations incorporate a phenomenological description of beam energy loss to explain the experimental data on DY yields [24–30]. In this region of x_t the nuclear modification of sea quark PDF and mesonic contributions also become important. Thus in this process, main nuclear effects are due to nuclear structure, mesonic contributions and shadowing (as in the case of DIS) with additional effect of parton energy loss in the beam parton energy due to the presence of nuclear targets.

In this paper, we present the results of nuclear medium effects on DY production of lepton pairs calculated in a

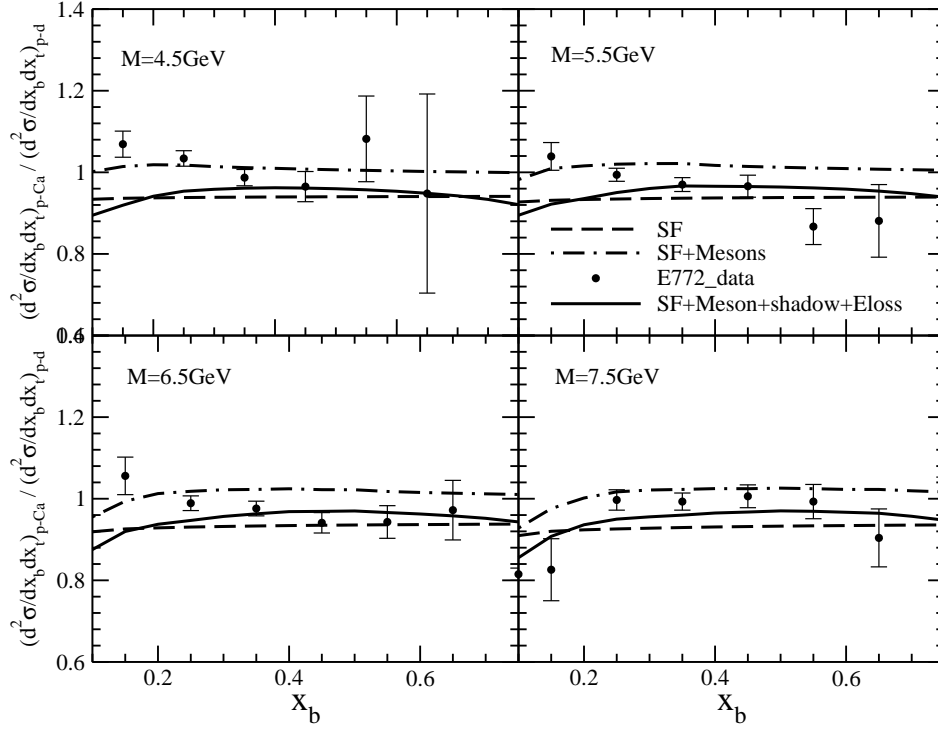


FIG. 3: $\frac{(\frac{d\sigma}{dx_b dx_t})_{p-Ca}}{(\frac{d\sigma}{dx_b dx_t})_{p-D}}^{40}$ vs x_b at $E=800\text{GeV}(\sqrt{s_N}=38.8\text{GeV})$. Lines and points have the same meaning as in Fig.2

microscopic nuclear model which has been successfully used to describe the DIS of charged leptons and $\nu/\bar{\nu}$ from various nuclei [31–36]. The model uses a relativistic nucleon spectral function to describe target nucleon momentum distribution incorporating Fermi motion, binding energy effects and nucleon correlations in a field theoretical model. The model has also been used to include the mesonic contributions from π and ρ mesons. The beam energy loss has been calculated using some phenomenological models discussed in the literature [24]–[30]. The results have been presented for the kinematic region of experiments E772 [37] and E866 [30, 38] or proton induced DY processes in nuclear targets like ^9Be , ^{12}C , ^{40}Ca , ^{56}Fe and ^{184}W in the region of $x_t > 0.1$. The numerical results extended up to $x_t = 0.45$, should be useful in analyzing the forthcoming experimental results from the SeaQuest E906 experiment being done at Fermi Lab [39].

In section-II, we present the formalism in brief; in section-III, the results are presented and discussed; and finally in section-IV, we summarize the results and conclude our findings.

II. NUCLEAR EFFECTS

When DY process takes place in nuclei, nuclear effects appear which are generally believed to be due to

- (a) nuclear structure effects arising from Fermi motion, binding energy and nucleon correlations,
- (b) additional contribution due to subnucleonic degrees of freedom like mesons and/or quark clusters in the nuclei,
- (c) shadowing effect, and
- (d) energy loss of the beam proton as it traverses the nuclear medium before producing lepton pairs.

In the case of proton induced DY processes in nuclei, the target nucleon has a Fermi momentum described by a momentum distribution. The target Bjorken variable x_t is defined for a free nucleon as $x_t = \frac{2q \cdot p_1}{(p_1 + p_2)^2}$, where q is the four momentum of $\mu^+ \mu^-$ pair, $p_{1\mu}$ and $p_{2\mu}$ are respectively the beam and target four momenta in the nuclear medium. Moreover, the projectile Bjorken variable x_b expressed covariantly as $x_b = \frac{2q \cdot p_2}{(p_1 + p_2)^2}$ also changes due to the energy loss of the beam particle caused by the initial state interactions with the nuclear constituents as it travels through the nuclear medium before producing lepton pairs. These nuclear modifications are incorporated while evaluating Eq.(1). Furthermore, there are additional contributions from the pion and rho mesons which are also taken into account.

In the following, we briefly outline the model and refer to earlier work [23, 31, 32] for details.

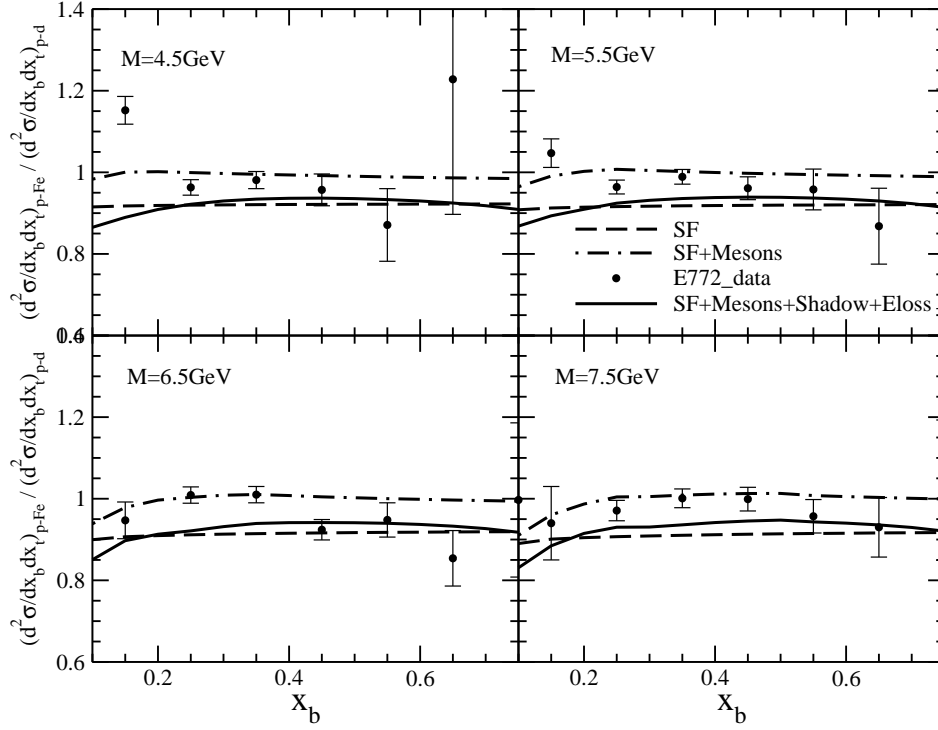


FIG. 4: $\frac{(\frac{d\sigma}{dx_b dx_t})_{p-Fe}}{(\frac{d\sigma}{dx_b dx_t})_{p-D}} \text{ vs } x_b$ at $E=800\text{GeV}(\sqrt{s_N}=38.8\text{GeV})$. Lines and points have the same meaning as in Fig.2

A. Nuclear Structure

In a nucleus, scattering is assumed to take place from partons inside the individual nucleons which are bound and moving with a momentum \vec{p} within a limit given by the Fermi momentum. The target Bjorken variable x_t becomes Fermi momentum dependent and PDF for quarks and antiquarks in the nucleus i.e. $q_f^t(x_t)$ and $\bar{q}_f^t(x_t)$ are calculated as a convolution of the PDFs in bound nucleon and a momentum distribution function of the nucleon inside the nucleus. The parameters of the momentum distribution are adjusted to correctly incorporate nuclear properties like binding energy, Fermi motion and the nucleon correlation effects in the nuclear medium. We use the Lehmann representation of the relativistic Dirac propagator for an interacting Fermi sea in nuclear matter to derive such a momentum distribution and Local Density Approximation to translate these results for a finite nucleus [23, 32–35]. The free relativistic propagator for a nucleon of mass M_N is written in terms of positive and negative energy components as

$$G^0(p_0, \mathbf{p}) = \frac{M_N}{E(\mathbf{p})} \left\{ \frac{\sum_r u_r(\mathbf{p}) \bar{u}_r(\mathbf{p})}{p^0 - E(\mathbf{p}) + i\epsilon} + \frac{\sum_r v_r(-\mathbf{p}) \bar{v}_r(-\mathbf{p})}{p^0 + E(\mathbf{p}) - i\epsilon} \right\} \quad (2)$$

For a noninteracting Fermi sea where only positive energy solutions are considered the relevant propagator is rewritten in terms of occupation number $n(\mathbf{p}) = 1$ for $p \leq p_F$ while $n(\mathbf{p})=0$ for $p > p_F$:

$$G^0(p_0, \mathbf{p}) = \frac{M_N}{E(\mathbf{p})} \left\{ \sum_r u_r(\mathbf{p}) \bar{u}_r(\mathbf{p}) \left[\frac{1 - n(\mathbf{p})}{p^0 - E(\mathbf{p}) + i\epsilon} + \frac{n(\mathbf{p})}{p^0 - E(\mathbf{p}) - i\epsilon} \right] \right\} \quad (3)$$

The nucleon propagator in an interacting Fermi sea is then calculated by making a perturbative expansion of $G(p_0, \mathbf{p})$ in terms of free nucleon propagator $G^0(p_0, \mathbf{p})$ given in Eq. (2) by retaining the positive energy contributions only (the negative energy components are suppressed).

This perturbative expansion is then summed in ladder approximation to give dressed nucleon propagator $G(p_0, \mathbf{p})$

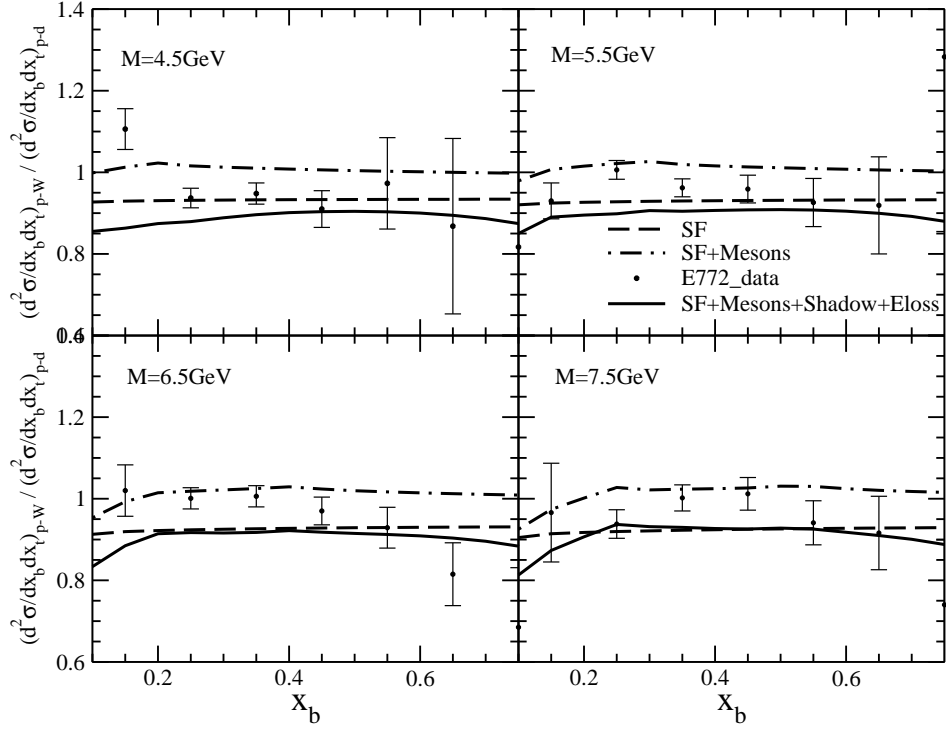


FIG. 5: $\frac{(\frac{d\sigma}{dx_b \frac{d\sigma}{dx_t}})_{p-^{184}W}}{(\frac{d\sigma}{dx_b \frac{d\sigma}{dx_t}})_{p-^2D}}$ vs x_b at $E=800\text{GeV}(\sqrt{s_N}=38.8\text{GeV})$. Lines and points have the same meaning as in Fig.2

[31, 40]

$$\begin{aligned}
 G(p_0, \mathbf{p}) &= \frac{M_N}{E(\mathbf{p})} \sum_r u_r(\mathbf{p}) \bar{u}_r(\mathbf{p}) \frac{1}{p^0 - E(\mathbf{p})} + \frac{M_N}{E(\mathbf{p})} \sum_r \frac{u_r(\mathbf{p}) \bar{u}_r(\mathbf{p})}{p^0 - E(\mathbf{p})} \sum(p^0, \mathbf{p}) \frac{M_N}{E(\mathbf{p})} \sum_s \frac{u_s(\mathbf{p}) \bar{u}_s(\mathbf{p})}{p^0 - E(\mathbf{p})} + \dots \\
 &= \frac{M_N}{E(\mathbf{p})} \frac{\sum_r u_r(\mathbf{p}) \bar{u}_r(\mathbf{p})}{p^0 - E(\mathbf{p}) - \sum(p^0, \mathbf{p}) \frac{M_N}{E(\mathbf{p})}},
 \end{aligned} \tag{4}$$

where $\sum(p^0, \mathbf{p})$ is the nucleon self energy.

This allows us to write the relativistic nucleon propagator in a nuclear medium in terms of the Spectral functions of hole and particle as [40]

$$G(p^0, \mathbf{p}) = \frac{M_N}{E(\mathbf{p})} \sum_r u_r(\mathbf{p}) \bar{u}_r(\mathbf{p}) \left[\int_{-\infty}^{\mu} d\omega \frac{S_h(\omega, \mathbf{p})}{p^0 - \omega - i\eta} + \int_{\mu}^{\infty} d\omega \frac{S_p(\omega, \mathbf{p})}{p^0 - \omega + i\eta} \right] \tag{5}$$

where $S_h(\omega, \mathbf{p})$ and $S_p(\omega, \mathbf{p})$ being the hole and particle spectral functions respectively, which are derived in Ref. [40], and μ is the chemical potential. We use:

$$S_h(p^0, \mathbf{p}) = \frac{1}{\pi} \frac{\frac{M_N}{E(\mathbf{p})} \text{Im}\Sigma(p^0, \mathbf{p})}{(p^0 - E(\mathbf{p}) - \frac{M_N}{E(\mathbf{p})} \text{Re}\Sigma(p^0, \mathbf{p}))^2 + (\frac{M_N}{E(\mathbf{p})} \text{Im}\Sigma(p^0, \mathbf{p}))^2} \tag{6}$$

for $p^0 \leq \mu$

$$S_p(p^0, \mathbf{p}) = -\frac{1}{\pi} \frac{\frac{M_N}{E(\mathbf{p})} \text{Im}\Sigma(p^0, \mathbf{p})}{(p^0 - E(\mathbf{p}) - \frac{M_N}{E(\mathbf{p})} \text{Re}\Sigma(p^0, \mathbf{p}))^2 + (\frac{M_N}{E(\mathbf{p})} \text{Im}\Sigma(p^0, \mathbf{p}))^2} \tag{7}$$

for $p^0 > \mu$.

The normalization of this spectral function is obtained by imposing the baryon number conservation following the method of Frankfurt and Strikman [41]. In the present paper, we use local density approximation (LDA) where we

do not have a box of constant density, and the reaction takes place at a point \mathbf{r} , lying inside a volume element d^3r with local density $\rho_p(\mathbf{r})$ and $\rho_n(\mathbf{r})$ corresponding to the proton and neutron densities at the point \mathbf{r} . This leads to the spectral functions for the protons and neutrons to be the function of local Fermi momentum given by

$$k_{F_p}(\mathbf{r}) = [3\pi^2\rho_p(\mathbf{r})]^{1/3}, \quad k_{F_n}(\mathbf{r}) = [3\pi^2\rho_n(\mathbf{r})]^{1/3} \quad (8)$$

and therefore the normalization condition may be imposed as

$$2 \int \frac{d^3p}{(2\pi)^3} \int_{-\infty}^{\mu_{p(n)}} S_h^{p(n)}(\omega, \mathbf{p}, k_{F_{p,n}}(\mathbf{r})) d\omega = \rho_{p,n}(\mathbf{r}), \quad (9)$$

where the factor of two is to take into account spin degrees of freedom of proton and neutron, and μ_p and μ_n are the chemical potentials for proton and neutron respectively.

This further leads to the normalization condition given by

$$2 \int d^3r \int \frac{d^3p}{(2\pi)^3} \int_{-\infty}^{\mu_{p(n)}} S_h^{p(n)}(\omega, \mathbf{p}, \rho_{p(n)}(\mathbf{r})) d\omega = Z(N), \quad (10)$$

The average kinetic and total nucleon energy in a nucleus with the same number of protons and neutrons are given by:

$$\langle T \rangle = \frac{4}{A} \int d^3r \int \frac{d^3p}{(2\pi)^3} (E(\mathbf{p}) - M_N) \int_{-\infty}^{\mu} S_h(p^0, \mathbf{p}, \rho(r)) dp^0, \quad (11)$$

$$\langle E \rangle = \frac{4}{A} \int d^3r \int \frac{d^3p}{(2\pi)^3} \int_{-\infty}^{\mu} S_h(p^0, \mathbf{p}, \rho(r)) p^0 dp^0, \quad (12)$$

where $\rho(r)$ is the baryon density for the nucleus which is normalized to A and is taken from the electron nucleus scattering experiments. The binding energy per nucleon is given by [31]:

$$|E_A| = -\frac{1}{2}(\langle E - M_N \rangle + \frac{A-2}{A-1} \langle T \rangle) \quad (13)$$

The binding energy per nucleon for each nucleus is correctly reproduced to match with the experimentally observed values. Once the spectral function is normalized to the number of nucleons and we obtain the correct binding energy, there is no free parameter that is left in our model.

In the case of nucleus, the nuclear hadronic tensor $W_A^{\mu\nu}$ for an isospin symmetric nucleus is derived to be [31, 32]:

$$W_A^{\mu\nu} = 2 \sum_{i=p,n} \int d^3r \int \frac{d^3p}{(2\pi)^3} \frac{M_N}{E(\mathbf{p})} \int_{-\infty}^{\mu} dp^0 S_h(p^0, \mathbf{p}, \rho_i) W_i^{\mu\nu}(p, q) \quad (14)$$

Using this, the electromagnetic structure function $F_{2A}(x, Q^2)$ for a non-symmetric (N \neq Z) nucleus in DIS is obtained as [31],

$$F_{2A}(x, Q^2) = 2 \sum_{i=p,n} \int d^3r \int \frac{d^3p}{(2\pi)^3} \frac{M_N}{E(\mathbf{p})} \int_{-\infty}^{\mu_i} dp^0 S_h^i(p^0, \mathbf{p}, \rho_i(r)) \sum_f e_f^2 x'_t [q_f^i(x'_t(p^0, \vec{p})) + \bar{q}_f^i(x'_t(p^0, \vec{p}))] \quad (15)$$

For the numerical calculations, we have used CTEQ6.6 [42] nucleon parton distribution functions(PDFs) for quark(q_f^i) and antiquark(\bar{q}_f^i) of flavor f.

Following the same procedure as taken for the evaluation of nuclear structure function, we incorporate the nuclear medium effects like Fermi motion, binding energy and nucleon correlations in the evaluation of bound quarks in nucleons of a nucleus. $q_f^i(x_t)$ and $\bar{q}_f^i(x_t, Q^2)$ are expressed in terms of spectral function as [23]:

$$\begin{aligned} q_f^i(x_t, Q^2) &= 2 \sum_{i=p,n} \int d^3r \int \frac{d^3p}{(2\pi)^3} \frac{M_N}{E(\mathbf{p})} \int_{-\infty}^{\mu_i} dp^0 S_h^i(p^0, \mathbf{p}, \rho_i(r)) q_f^i(x'_t(p^0, \vec{p}), Q^2) \\ \bar{q}_f^i(x_t, Q^2) &= 2 \sum_{i=p,n} \int d^3r \int \frac{d^3p}{(2\pi)^3} \frac{M_N}{E(\mathbf{p})} \int_{-\infty}^{\mu_i} dp^0 S_h^i(p^0, \mathbf{p}, \rho_i(r)) \bar{q}_f^i(x'_t(p^0, \vec{p}), Q^2), \end{aligned} \quad (16)$$

where $q_f^i(\bar{q}_f^i(x_t, Q^2))$ is the quark(antiquark) PDFs for flavor f inside a nucleon of kind i and the factor of 2 is because of quark(antiquark) spin degrees of freedom. $x_t' = \frac{M_N}{p^0 - p_z} x_t$ which is obtained from the covariant expression of $x_t' = \frac{q \cdot p_1}{s_N}$ with $q||z$ direction.

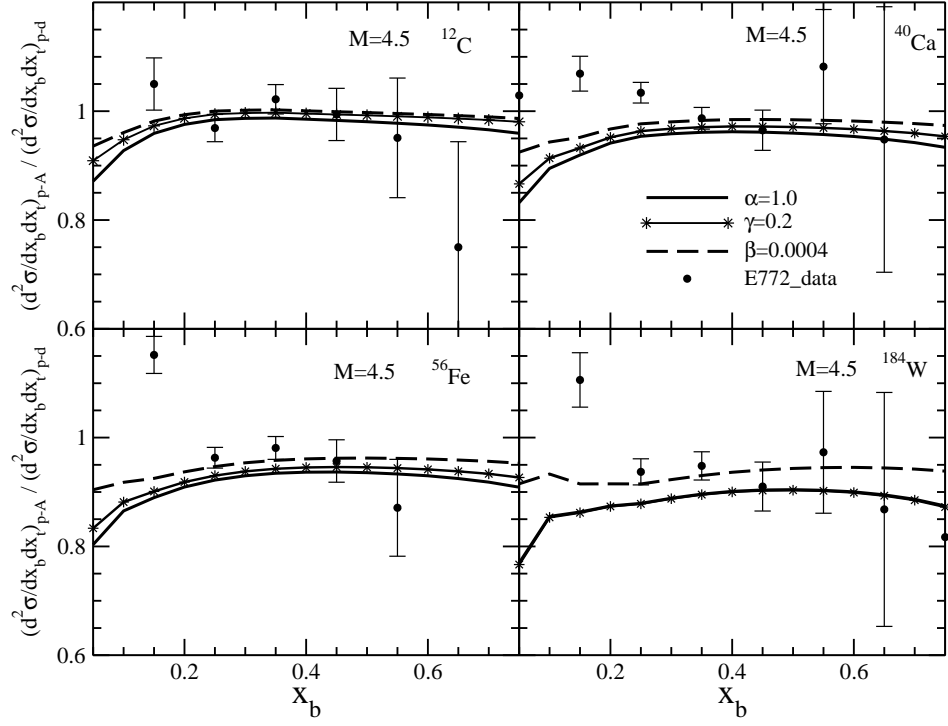


FIG. 6: $\frac{(\frac{d\sigma}{dx_b dx_t})_{p-A}}{(\frac{d\sigma}{dx_b dx_t})_{p-d}}$ vs x_b at $E=800\text{GeV}(\sqrt{s_N}=38.8\text{GeV})$. The results are obtained using the full model at $M=4.5\text{GeV}$. 'A' stands for several nuclei like ^{12}C , ^{40}Ca , ^{56}Fe and ^{184}W . These results are obtained using different models for the energy loss viz. $\alpha = 1$ in Eq.(27) shown by the solid line, $\gamma = 0.2$ in Eq.(28) shown by the solid line with stars and $\beta = 0.0004$ in Eq.(29) shown by the dashed line. Experimental points are data of E772 experiment [37, 49].

B. Mesonic contributions

As the nucleons are strongly interacting particles and inside the nucleus continuous exchange of virtual mesons take place, therefore, we have also taken into account the probability of interaction of virtual photons with the meson clouds. In the present work, we have considered π and ρ mesons. For this the imaginary part of the meson propagators are introduced instead of spectral function which were derived from the imaginary part of the nucleon propagator. Therefore, in the case of pion, we replace in Eq.(15) [32]:

$$\frac{M_N}{E(\mathbf{p})} \int_{-\infty}^{\mu} d\omega S_h(\omega, \mathbf{p}) \delta(p^0 - \omega) \rightarrow -\frac{1}{\pi} \theta(p_0) \text{Im} D(p)$$

where $D(p)$ is the pion propagator in the nuclear medium given by

$$D(p) = [p^{02} - \vec{p}^2 - m_\pi^2 - \Pi_\pi(p^0, \mathbf{p})]^{-1}, \quad (17)$$

with

$$\Pi_\pi = \frac{f^2/m_\pi^2 F^2(p) \vec{p}^2 \Pi^*}{1 - f^2/m_\pi^2 V_L' \Pi^*}. \quad (18)$$

Here, $F(p) = (\Lambda_\pi^2 - m_\pi^2)/(\Lambda_\pi^2 + \vec{p}^2)$ is the πNN form factor, $\Lambda_\pi=1\text{GeV}$, $f = 1.01$, V_L' is the longitudinal part of the spin-isospin interaction and Π^* is the irreducible pion self energy that contains the contribution of particle - hole and delta - hole excitations.

Following a similar procedure, as done in the case of nucleon, the contribution of the pions to hadronic tensor in the nuclear medium may be written as [31]

$$W_{A,\pi}^{\mu\nu} = 3 \int d^3r \int \frac{d^4p}{(2\pi)^4} \theta(p^0) (-2) \text{Im} D(p) 2m_\pi W_\pi^{\mu\nu}(p, q) \quad (19)$$

However, Eq.(19) also contains the contribution of the pionic contents of the nucleon, which are already contained in the sea contribution of nucleon through Eq.(16), therefore, the pionic contribution of the nucleon is to be subtracted from Eq.(19), in order to calculate the contribution from the excess pions in the nuclear medium. This is obtained by replacing $ImD(p)$ by $\delta ImD(p)$ [31] as

$$ImD(p) \rightarrow \delta ImD(p) \equiv ImD(p) - \rho \frac{\partial ImD(p)}{\partial \rho} \Big|_{\rho=0} \quad (20)$$

Using Eq.(19), pion structure function $F_{2,\pi}^A(x)$ in a nucleus is derived as

$$F_{2,\pi}^A(x) = -6 \int d^3r \int \frac{d^4p}{(2\pi)^4} \theta(p^0) \delta ImD(p) \frac{x}{x_\pi} 2M_N \sum_f e_f^2 x_\pi [q_\pi^f(x_\pi(p^0, \vec{p})) + \bar{q}_\pi^f(x_\pi(p^0, \vec{p}))] \theta(x_\pi - x) \theta(1 - x_\pi), \quad (21)$$

where $\frac{x}{x_\pi} = \frac{-p^0 + p^z}{M_N}$.

This in turn leads to the expression for the pion quark PDF in the nuclear medium. For example, $q_{f,\pi}^t(x_t, Q^2)$ is derived as [23]:

$$q_{f,\pi}^t(x_t, Q^2) = -6 \int d^3r \int \frac{d^4p}{(2\pi)^4} \theta(p^0) \delta ImD(p) 2M_N q_{f,\pi}(x_\pi) \theta(x_\pi - x_t) \theta(1 - x_\pi). \quad (22)$$

and a similar expression for $\bar{q}_{f,\pi}^t(x_t, Q^2)$.

Similarly, the contribution of the ρ -meson cloud to the structure function is taken into account in analogy with the above prescription and the rho structure function is written as [31]

$$F_{2,\rho}^A(x) = -12 \int d^3r \int \frac{d^4p}{(2\pi)^4} \theta(p^0) \delta ImD_\rho(p) \frac{x}{x_\rho} 2M_N \sum_f e_f^2 x_\rho [q_\rho^f(x_\rho(p^0, \vec{p})) + \bar{q}_\rho^f(x_\rho(p^0, \vec{p}))] \theta(1 - x_\rho) \theta(x_\rho - x) \quad (23)$$

and the expression for the rho PDF $q_{f,\rho}^t(x_t, Q^2)$ is derived as [23]:

$$q_{f,\rho}^t(x_t, Q^2) = -12 \int d^3r \int \frac{d^4p}{(2\pi)^4} \theta(p^0) \delta ImD_\rho(p) 2M_N q_{f,\rho}(x_\rho) \theta(x_\rho - x_t) \theta(1 - x_\rho), \quad (24)$$

where $D_\rho(p)$ is now the ρ -meson propagator in the nuclear medium given by:

$$D_\rho(p) = [p^{02} - \vec{p}^2 - m_\rho^2 - \Pi_\rho^*(p^0, \mathbf{p})]^{-1}, \quad (25)$$

where

$$\Pi_\rho^* = \frac{f^2/m_\pi^2 C_\rho F_\rho^2(p) \vec{p}^2 \Pi^*}{1 - f^2/m_\pi^2 V_T' \Pi^*}. \quad (26)$$

Here, V_T' is the transverse part of the spin-isospin interaction, $C_\rho = 3.94$, $F_\rho(p) = (\Lambda_\rho^2 - m_\rho^2)/(\Lambda_\rho^2 + \vec{p}^2)$ is the ρNN form factor, $\Lambda_\rho = 1\text{GeV}$, $f = 1.01$, and Π^* is the irreducible rho self energy that contains the contribution of particle - hole and delta - hole excitations and $\frac{x}{x_\rho} = \frac{-p^0 + p^z}{M_N}$. Quark and antiquark PDFs for pions have been taken from the parameterization given by Gluck et al.[43] and for the rho mesons we have taken the same PDFs as for the pions. It must be pointed out that the choice of Λ_π and $\Lambda_\rho (=1\text{GeV})$ in πNN and ρNN form factors have been fixed in our earlier works[32, 35, 36] while describing nuclear medium effects in electromagnetic structure function $F_2^{EM}(x, Q^2)$ to explain the latest data from JLab and other experiments performed using charged lepton beams on several nuclear targets.

We have also taken into account shadowing effect which arises due to coherent multiple scattering interactions of the intermediate states, which is important in DY production at small x_t . Various theoretical calculations have indicated that shadowing in DIS as well as in DY processes has a common origin. For the shadowing effect we have followed the model of Kulagin and Petti [8, 9].

C. Energy loss of beam partons

The incident proton beam traverses the nuclear medium before the beam parton undergoes a hard collision with the target parton. The incident proton may lose energy due to soft inelastic collisions as it might scatter on its way within the nucleus before producing a lepton pair.

There are many papers in literature [8, 23–28, 30, 44–47] where the effect of energy loss on DY process is discussed and models are given to incorporate them in the calculation of DY yields. However, there is no model which has the preference over the others. Most of them perform phenomenological fits and the best value of the parameters are those which have been obtained in the independent analysis of the experimental data. The present situation is summarized by Accardi et al.[47].

For example Duan et al. [24, 44, 45] have used two different kinds of quark energy loss expression, in which the fractional parton energy x_b is modified to $x_b \rightarrow x_b + \Delta x_b$, where in the linear fit Δx_b are given by

$$\Delta x_b = \alpha \frac{\langle L \rangle_A}{E_p}, \quad (27)$$

and by

$$\Delta x_b = \gamma \frac{\langle L \rangle_A^2}{E_p}. \quad (28)$$

where $\langle L \rangle_A = [3/4(1.2A^{1/3})]$ fm is the average path length of the incident quark in the nucleus A, E_p is the energy of the incident proton. The constants α and γ are varied to get a good fit with the experimental data which were found to be in the range of $1.27 \leq \alpha \leq 1.99$ GeV/fm and $0.2 \leq \gamma \leq 0.3$ GeV/fm² [8, 24–26, 30, 44, 45].

Gavin and Milana [46] have parameterized the energy loss effect as

$$\Delta x_b = \beta x_b A^{\frac{1}{3}}, \quad (29)$$

where $\beta = 0.0004$. However, in some recent work of Johnson et al. [25], Garvey and Peng [28], and Kulagin and Petti [8], it has been pointed out that a quantitative estimate of energy loss effect in DY processes depends upon how the shadowing effect is treated. In the presence of shadowing effect, the fitted parameter for energy loss alpha in equation 27 is found to be somewhat smaller in the range of 0.7 to 1.27.

D. Drell-Yan cross sections with nuclear effects

We have taken into account the various nuclear effects discussed above in this section and write the cross section for the DY process as

$$\frac{d^2\sigma^{(A)}}{dx_b dx_t} = \frac{d^2\sigma^{(SF)}}{dx_b dx_t} + \frac{d^2\sigma^{(\pi)}}{dx_b dx_t} + \frac{d^2\sigma^{(\rho)}}{dx_b dx_t}, \quad (30)$$

where $\frac{d^2\sigma^{(SF)}}{dx_b dx_t}$ is the DY cross section from the nucleons in the nucleus after incorporating the nuclear medium effects like Fermi motion, binding energy, nucleon correlations through the use of spectral function. Furthermore, we have also incorporated shadowing effect following Kulagin and Petti [8] and energy loss effect following the phenomenological model given in Eq. 27 with $\alpha=1$. The expression for $\frac{d^2\sigma^{(SF)}}{dx_b dx_t}$ is given by:

$$\begin{aligned} \frac{d^2\sigma^{(SF)}}{dx_b dx_t} = & \frac{4\pi\alpha^2}{9q^2} 4 \int d^3r \sum_f e_f^2 \left[q_{f,p}(x_b) \int \frac{d^3p}{(2\pi)^3} \frac{M_N}{E(\vec{p})} \int_{-\infty}^{\mu} dp^0 S_h(p^0, \mathbf{p}) \bar{q}_{f,N}(x'_t) \right. \\ & \left. + \bar{q}_{f,p}(x_b) \int \frac{d^3p}{(2\pi)^3} \frac{M_N}{E(\vec{p})} \int_{-\infty}^{\mu} dp^0 S_h(p^0, \mathbf{p}) q_{f,N}(x'_t) \right] \theta(x'_t) \theta(1-x'_t) \theta(1-x_b) \end{aligned} \quad (31)$$

where $S_h(p^0, \mathbf{p})$ is the hole spectral function for the nucleon in the nucleus. $q_{f,N} = \frac{1}{2}(q_{f,p} + q_{f,n})$ and $\bar{q}_{f,N} = \frac{1}{2}(\bar{q}_{f,p} + \bar{q}_{f,n})$ are the nucleon PDFs of flavor f averaged over proton and neutron in the cases of quarks and anti-quarks, respectively.

Similarly to include the pionic contribution $\frac{d^2\sigma^{(\pi)}}{dx_b dx_t}$ and the rho contribution $\frac{d^2\sigma^{(\rho)}}{dx_b dx_t}$, the DY cross sections are respectively written as [23]:

$$\begin{aligned} \frac{d^2\sigma^{(\pi)}}{dx_b dx_t} = & \frac{4\pi\alpha^2}{9q^2} (-6) \int d^3r \sum_f e_f^2 \left[q_{f,p}(x_b) \int \frac{d^4p}{(2\pi)^4} \theta(p^0) \delta \text{Im} D(p) 2M_N \bar{q}_{f,\pi}(x_\pi) \right. \\ & \left. + \bar{q}_{f,p}(x_b) \int \frac{d^4p}{(2\pi)^4} \theta(p^0) \delta \text{Im} D(p) 2M_N q_{f,\pi}(x_\pi) \right] \theta(x_\pi - x_t) \theta(1-x_\pi) \theta(1-x_b) \end{aligned} \quad (32)$$

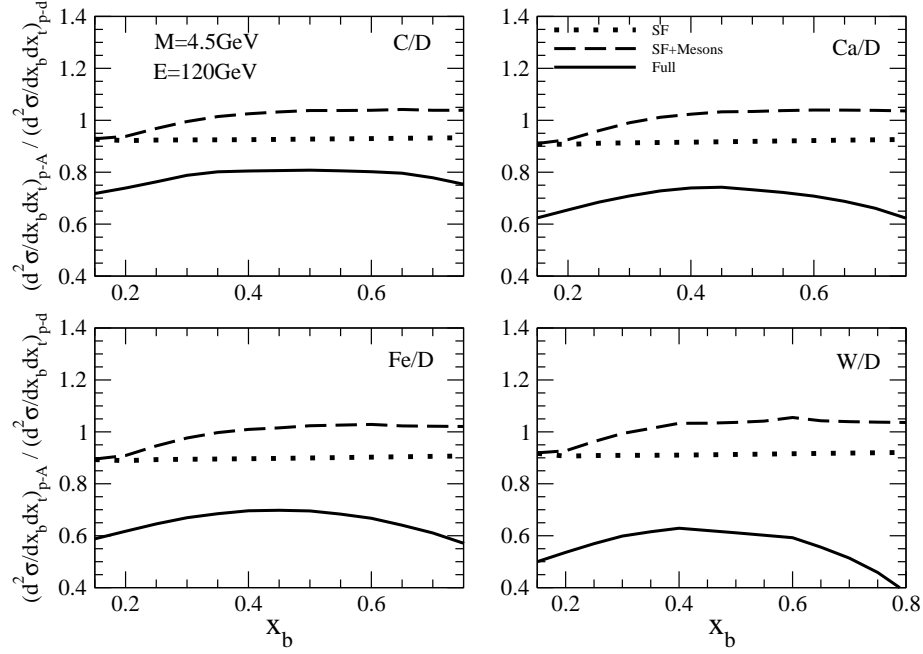


FIG. 7: $\frac{(\frac{d\sigma}{dx_b dx_t})_{p-A}}{(\frac{d\sigma}{dx_b dx_t})_{p-d}}$ vs x_b at $M = 4.5\text{GeV}$ for $A = {}^{12}\text{C}$, ${}^{40}\text{Ca}$, ${}^{56}\text{Fe}$ and ${}^{184}\text{W}$. For the beam energy $E=120\text{GeV}$ ($\sqrt{s_N}=15\text{GeV}$) the results are obtained with Spectral function: dotted line, including the mesonic contribution: dashed line, and for the full calculation: solid line.

and

$$\begin{aligned} \frac{d^2\sigma^{(\rho)}}{dx_b dx_t} = & \frac{4\pi\alpha^2}{9q^2}(-12) \int d^3r \sum_f e_f^2 \left[q_{f,p}(x_b) \int \frac{d^4p}{(2\pi)^4} \theta(p^0) \delta \text{Im} D_\rho(p) 2M_N \bar{q}_{f,\rho}(x_\rho) \right. \\ & \left. + \bar{q}_{f,p}(x_b) \int \frac{d^4p}{(2\pi)^4} \theta(p^0) \delta \text{Im} D_\rho(p) 2M_N q_{f,\rho}(x_\rho) \right] \theta(x_\rho - x_t) \theta(1 - x_\rho) \theta(1 - x_b) \end{aligned} \quad (33)$$

Since in the various experiments the DY cross sections are also obtained in terms of other variables like M , x_f , τ , etc, where, $M = \sqrt{x_b x_t s_N}$, $x_f = x_b - x_t$, $\tau = x_b x_t$, therefore, we have also obtained DY cross sections in terms of some of these variables. For example, using Jacobian transformation Eq.(31) may be written as:

$$\begin{aligned} \frac{d^2\sigma}{dx_b dM} = & \frac{8\pi\alpha^2}{9M} \frac{1}{x_b s_N} 4 \int d^3r \sum_f e_f^2 \left[q_{f,p}(x_b) \int \frac{d^3p}{(2\pi)^3} \frac{M_N}{E(\vec{p})} \int_{-\infty}^{\mu} dp^0 S_h(p^0, \mathbf{p}) \bar{q}_{f,N}(x'_t) \right. \\ & \left. + \bar{q}_{f,p}(x_b) \int \frac{d^3p}{(2\pi)^3} \frac{M_N}{E(\vec{p})} \int_{-\infty}^{\mu} dp^0 S_h(p^0, \mathbf{p}) q_{f,N}(x'_t) \right] \theta(x'_t) \theta(1 - x'_t) \theta(1 - x_b) \end{aligned} \quad (34)$$

Most of the experimental results for the DY process have been presented in the form of $\frac{\frac{d\sigma}{dx_b dx_t}(A)}{\frac{d\sigma}{dx_b dx_t}(D)}$ i.e. the ratio of DY cross section in a nuclear target ($\frac{d\sigma}{dx_b dx_t}(A)$) to the DY cross section in deuteron ($\frac{d\sigma}{dx_b dx_t}(D)$). Therefore, to evaluate proton-deuteron DY cross section, we write

$$\frac{d\sigma^{pd}}{dx_b dx_t} = \frac{d\sigma^{pp}}{dx_b dx_t} + \frac{d\sigma^{pn}}{dx_b dx_t}. \quad (35)$$

and to take into account the deuteron effect, the quark/antiquark distribution function inside the deuteron target have been calculated using the same formula as for the nuclear structure function but performing the convolution with the deuteron wave function squared instead of using the spectral function. The deuteron wave function has been taken from the works of Lacombe et al. [48].

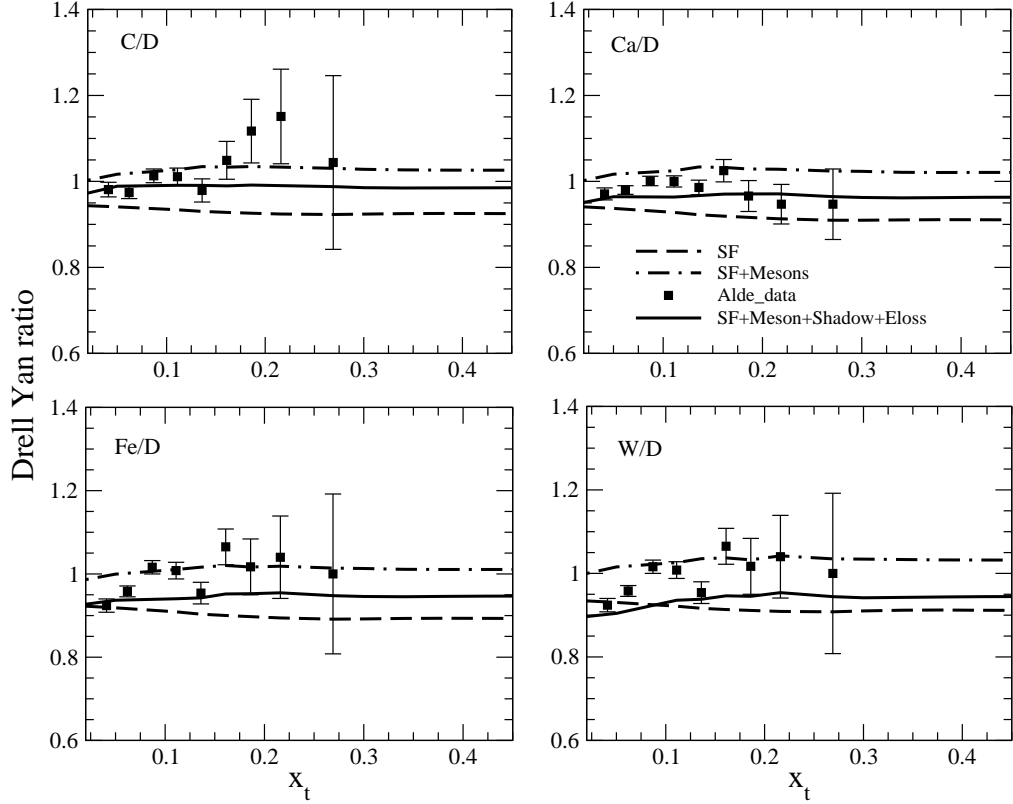


FIG. 8: Left panel: $\frac{\frac{d\sigma}{dx_t}(C, Fe)}{\frac{d\sigma}{dx_t}(D)}$ vs x_t at $E=800\text{GeV}$ ($\sqrt{s_N}=38.8\text{GeV}$), $x_b = x_t + 0.26$, $Q^2 > 16\text{GeV}^2$, with $\alpha = 1$ in Eq.(27). Spectral function: dashed line, including the mesonic contribution: dashed-dotted line, results of the full calculation: solid line. Experimental points are of E772 experiment [37]. Right panel: $\frac{\frac{d\sigma}{dx_t}(Ca, W)}{\frac{d\sigma}{dx_t}(D)}$ vs x_t , lines have same meaning as in the left panel.

In terms of the deuteron wave function, one may write

$$q_f^t(x_t, Q^2) = \int \frac{d^3p}{(2\pi)^3} \frac{M}{E_p^d} |\Psi_D(\mathbf{p})|^2 q_f^N(x'_t(\mathbf{p}), Q^2), \quad (36)$$

where the four momentum of the proton inside the deuteron is described by $p^\mu = (E_p^d, \mathbf{p})$ with $E_p^d (= M_{\text{Deuteron}} - \sqrt{M^2 + |\mathbf{p}|^2})$ as the energy of the off shell proton inside the deuteron and M_{Deuteron} is the deuteron mass. A similar expression has been used for the antiquarks $\bar{q}_f^t(x_t, Q^2)$.

III. RESULTS AND DISCUSSION

The results presented here are based on the following calculations:

- (1) DY cross section for proton-nucleus scattering i.e. $\left(\frac{d\sigma}{dx_b dx_t}\right)^A$, where A stands for a nuclear target, has been obtained by using the spectral function $S_h(p^0, \mathbf{p})$ which takes into account Fermi motion, nucleon correlations and binding energy. The spectral function with parameters fixed by Eqs.(9) and (10) has been used to calculate the nucleon contribution which reproduce mass number of the nucleon, the binding energy per nucleon for a given nucleus.
- (2) We add contributions obtained from the pion cloud using Eq.(32) and Eq.(33) for the rho meson to nucleon contributions. For evaluating the mesonic contributions the parameters of $D(p)$ in Eq.(17) and $D_\rho(p)$ in Eq.(25) are fixed by fitting experimental data on $F_2^i(x_t)$ in DIS on various nuclei [32, 35].
- (3) We have also included shadowing effect following the works of Kulagin and Petti [8]. With the inclusion of shadowing effect along with the spectral function and meson cloud contributions, the numerical results have been presented.

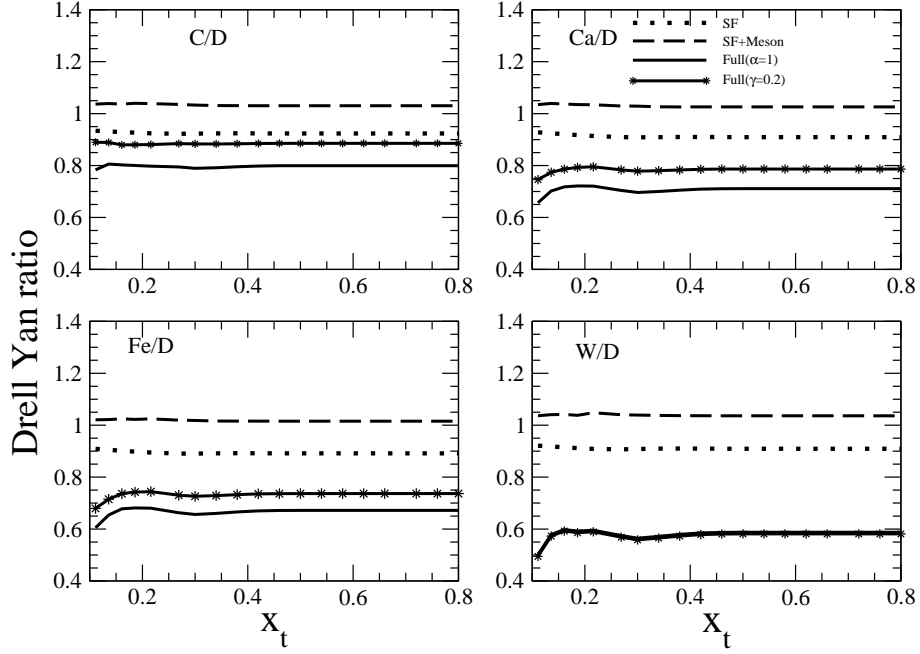


FIG. 9: Left panel: $\frac{d\sigma}{dx_t}(C, Fe)$ vs x_t at $E=120\text{GeV}(\sqrt{s_N}=15\text{GeV})$, $x_b = x_t + 0.26$, $Q^2 > 16\text{GeV}^2$. The results are obtained with Spectral function: dotted line, Spectral function+Mesonic contribution: dashed line. The results of our full calculations are obtained with energy loss using Eq.(27) with $\alpha = 1$ (solid line) and $\gamma = 0.2$ in Eq.(28) (solid line with stars). Right panel: $\frac{d\sigma}{dx_t}(Ca, W)$ vs x_t , lines have same meaning as in the left panel.

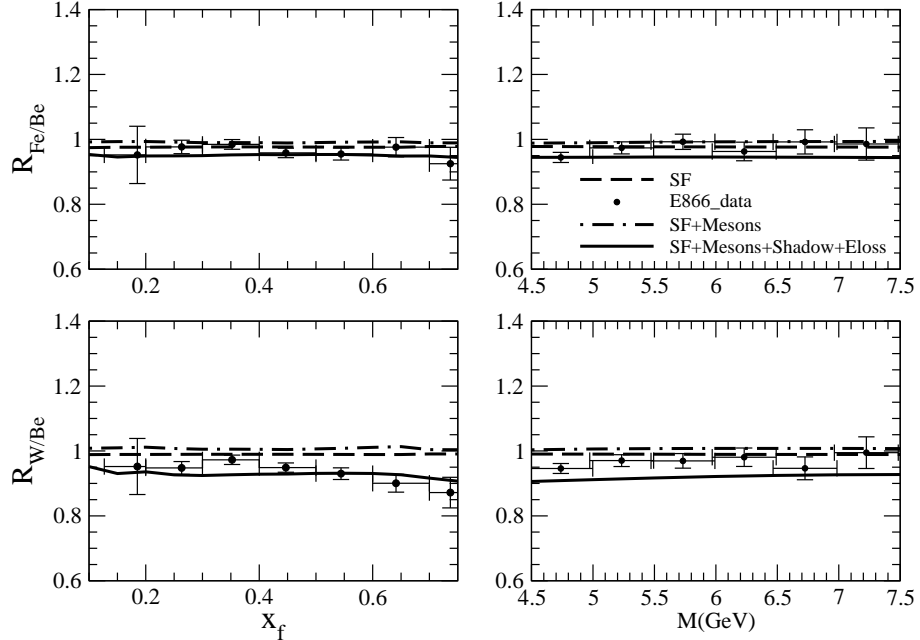


FIG. 10: Left Panel: $\frac{d\sigma}{dx_F}(Fe, W)$ vs x_F , Right Panel: $\frac{d\sigma}{dM}(Fe, W)$ vs $M(= \sqrt{x_b x_t s_N})\text{GeV}$, at $E=800\text{GeV}(\sqrt{s_N}=38.8\text{GeV})$, with $\alpha = 1$ in Eq.(27). Experimental points are of E866 experiment [30, 38] with $0.01 < x_t < 0.12$, $0.21 < x_b < 0.95$ and $0.13 < x_F < 0.93$. Spectral function: dashed line, including the mesonic contribution: dashed-dotted line, results of the full calculation: solid line.

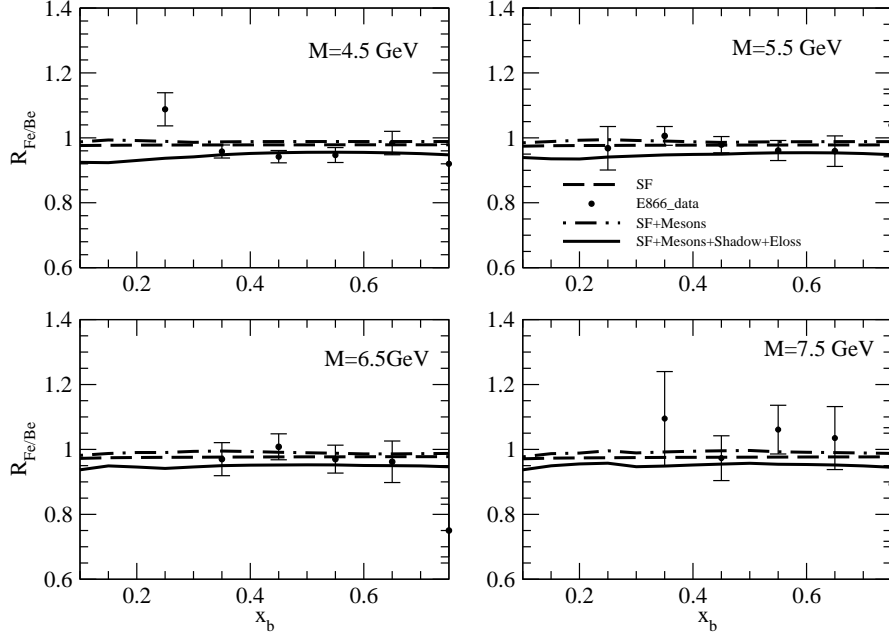


FIG. 11: $\frac{d\sigma}{dM dx_b}(Fe)$ vs x_b at different $M(=\sqrt{x_b x_t s_N})$ with $E=800\text{GeV}(\sqrt{s_N}=38.8\text{GeV})$, and $\alpha = 1$ in Eq.(27). Experimental points are of E866 experiment [30, 38]. Spectral function: dashed line, including the mesonic contribution: dashed-dotted line, results of the full calculation: solid line

(4) For the energy loss we have used Eq.(27) with $\alpha = 1$. There are other phenomenological models available in the literature to take into account the energy loss effect. We have, therefore, studied the dependence of DY cross sections on energy loss if one uses other phenomenological parameterizations. Some of the expressions are given in Eq.(28) and Eq.(29). For our numerical calculations we have taken $\gamma=0.2$. Also we have performed calculations using Eq.(29) with $\beta = 0.0004$.

(5) DY cross section for proton-deuteron scattering has been obtained using Eq.(35) and no energy loss effect has been taken in deuteron. We have obtained the results by using Eq.(36) with deuteron effect which has found to be small.

(6) For nucleon quark/antiquark PDFs CTEQ6.6 [42] has been used and for pion quark/antiquark PDFs parameterization of Gluck et al. [43] has been used.

In Figs.2-5, we present the results for the ratio $R = \frac{(\frac{d\sigma}{dx_b dx_t})_{p-A}}{(\frac{d\sigma}{dx_b dx_t})_{p-D}}$ vs x_b for $M=4.5, 5.5, 6.5$ and 7.5GeV . The center of mass energy ($\sqrt{s_N}$) is 38.8GeV . Here A is ^{12}C in Fig.2, ^{40}Ca in Fig.3, ^{56}Fe in Fig.4 and ^{184}W in Fig.5. These results are presented for the numerator obtained using the spectral function, including the mesonic effect, and also including shadowing and energy loss effect which is our full model. We find that the nuclear structure effects due to bound nucleon lead to a suppression in the DY yield of about 5 – 6% in ^{12}C in the region of $0.2 < x_b < 0.6$. This suppression increases with the increase in mass number of the nuclear target. For example, in ^{184}W it becomes 6 – 8% for $0.2 < x_b < 0.6$. Furthermore, we find that there is a significant contribution of mesons which increases the DY ratio i.e. its effect is opposite to the effect of spectral function. For example, the DY yield increases by around 6 – 8% for $0.2 < x_b < 0.6$ in ^{12}C . Moreover, we observe that the effect is more at low x_b ($\sim 0.2 - 0.3$) than at high x_b . This increase in the DY yield from meson cloud contribution also increases with the mass number A, for example in ^{184}W it is around 8 – 10% for $x_b = 0.2 - 0.3$. We find the contribution from rho meson cloud to be much smaller than the contribution from pion cloud.

When the shadowing corrections are included there is further suppression in the DY yield and it is effective in the low region of x_b . The effect of beam energy loss is also to reduce the DY yield. Both effects further adds to the suppression obtained using spectral function, where as mesonic effects lead to an enhancement. The net effect of shadowing and the energy loss effect is 7% at $x_b = 0.1$ in ^{12}C which becomes 4% at $x_b = 0.2$ for $M = 4.5\text{GeV}$. The shadowing effect as well as energy loss effect are more pronounced in heavier nuclei and suppresses the DY ratio considerably. For example, in ^{184}W at low x_b this suppression is about 14 – 15% at $x_b = 0.1 - 0.2$ which becomes 10% at $x_b = 0.3$. Moreover, the shadowing effect is M dependent, like in ^{184}W the total effect becomes about 10 – 12%

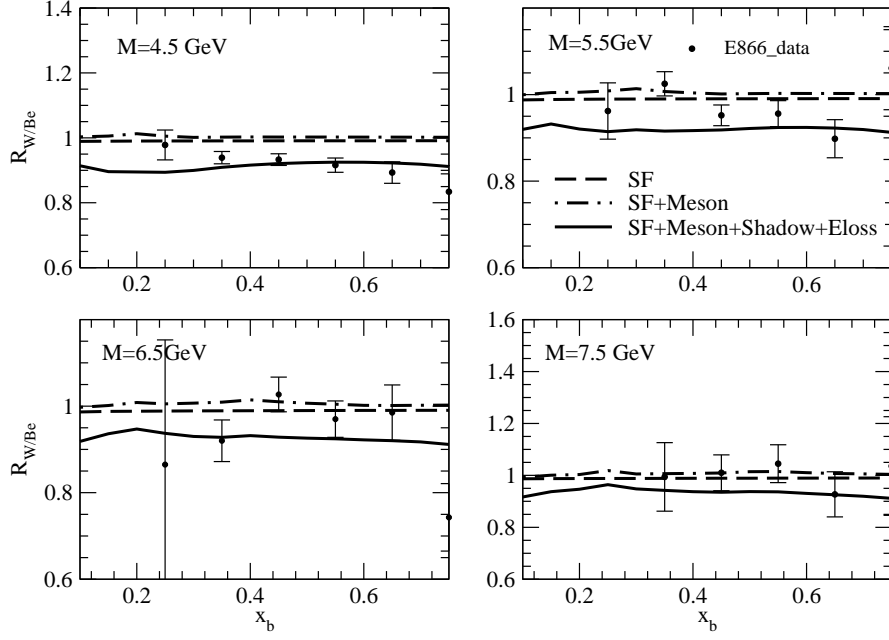


FIG. 12: $\frac{\frac{d\sigma}{dM dx_b}(W)}{\frac{d\sigma}{dM dx_b}(Be)}$ vs x_b at different $M(= \sqrt{x_b x_t s_N})$ with $\sqrt{s_N}=38.8\text{GeV}$, with $\alpha = 1$ in Eq.(27). Experimental points are of E866 experiment [30, 38]. Spectral function: dashed line, including the mesonic contribution: dashed-dotted line, results of the full calculation: solid line.

at $x_b = 0.1 - 0.2$ for $M = 7.5\text{GeV}$. It is observed that the suppression in the DY ratio due to energy loss effect (not shown in these figures) is $\sim 2 - 4\%$ in the case of ^{12}C which increases to $3 - 6\%$ in ^{40}Ca and ^{56}Fe , and becomes around $4 - 10\%$ in ^{184}W in the region of $x_b < 0.75$.

To observe the effect of energy loss using the various approaches, in Fig.6, we present the results of full calculation for $\frac{(\frac{d\sigma}{dx_b dx_t})_{p-A}}{(\frac{d\sigma}{dx_b dx_t})_{p-^2D}}$ at $M=4.5\text{GeV}$ and $\sqrt{s_N}=38.8\text{GeV}$ for $\alpha=1$ in Eq. (27), $\gamma=0.2$ in Eq. (28) and $\beta = 0.0004$ in Eq.(29).

We find that there is hardly any difference in the results obtained with $\gamma=0.2$ in Eq. (28) in comparison to the results obtained with $\alpha=1$ in Eq. (27). When we obtain the results using $\beta = 0.0004$ in Eq.(29), it is found that there is less reduction in the DY ratio for heavier nuclear targets like ^{184}W as compared to the results obtained using $\alpha=1$ in Eq. (27), while for the light nuclear targets the results are comparable. We have also studied(not shown here) the dependence of the parameter α used in the expression given in Eq.(27) for energy loss, we have varied α in the range

$0.5 < \alpha < 3$, corresponding to the range of values used in literature [24, 25, 44], for $\frac{(\frac{d\sigma}{dx_b dx_t})_{p-A}}{(\frac{d\sigma}{dx_b dx_t})_{p-^2D}}$ at $M=4.5\text{GeV}$

and $\sqrt{s_N}=38.8\text{GeV}$. We find that in the case of $p-^{12}\text{C}$ DY process, there is less(more) suppression when α is taken as $0.5(2)$ from the results obtained at $\alpha=1$, our reference value. For example, this is around $1 - 2\%$ lesser(larger) at $x_b \sim 0.1-0.2$ at $\alpha=0.5(2)$. With the increase in mass number the difference in the results increases. For example, in ^{184}W this suppression is around $2 - 3\%$ lesser(larger) at $x_b \sim 0.1-0.2$ at $\alpha=0.5(2)$. Thus we observe that with the increase in α , DY ratio decreases considerably and there is an 'A' dependence on the DY ratio. The numerical results are compared with the E772 experimental data and found to be in fair agreement.

To explicitly compare the effect of nuclear medium as well as energy loss in DY production cross section at different center of mass energies, in Fig. 7, we have presented the results for $\frac{\frac{d\sigma}{dx_b dx_t}(A)}{\frac{d\sigma}{dx_b dx_t}(D)}$ vs x_b at $M = 4.5\text{GeV}$ for $A = ^{12}\text{C}$, ^{40}Ca , ^{56}Fe and ^{184}W at $E=120\text{GeV}(\sqrt{s_N}=15\text{GeV})$. These results depict how the DY ratio vary at the different center of mass energies when the results are obtained with Spectral function, including mesonic contribution and the full calculation without energy loss and with energy loss for $\alpha = 1$ in Eq.(27). For $E=120\text{GeV}$, we observe that the effect of spectral function is to reduce DY yield by about 7% for ^{12}C and the reduction increases with the increase in mass number like for ^{184}W it is 9% . When the meson cloud contributions are included the DY yield get enhanced by $4 - 6\%$ at low x_b and $10 - 12\%$ at mid and high values of x_b and is found almost independent of A . When shadowing and energy loss effects are added, the results get reduced by $13 - 15\%$ in the range of $0.2 < x_b < 0.6$ and show significant reduction at high values of x_b which is around $16 - 28\%$ in ^{12}C . Furthermore, we observe a strong

nuclear mass dependence on the DY yield due to energy loss and shadowing effects, for example it is 45 – 50% for ^{184}W . When we compare the present results obtained using full model with the results obtained at $E=800\text{GeV}$ for $M=4.5\text{GeV}$ (Figs.2-5), it may be observed that the decrease in DY yield is mainly due to the large energy loss at low center of mass energy.

In Fig.8, we present the results for $\frac{(\frac{d\sigma}{dx_t})_{p-A}}{(\frac{d\sigma}{dx_t})_{p-^2D}}$ vs x_t at $\sqrt{s_N}=38.8\text{GeV}$ by integrating over x_b . The integration over x_b is done by putting the constraints as $x_F(=x_b-x_t) > 0.26$ and $Q^2 > 16\text{GeV}^2$. We find the effect of spectral function to be around 6 – 8% in ^{12}C which increases with mass number and becomes around 8 – 9% in ^{184}W , and is found to be almost independent of x_t . The addition of the mesonic contribution enhances the DY yield, for example, in ^{12}C this increase is 10 – 12% which further get enhances with increase in mass number and becomes around 12 – 14% in ^{184}W . When the results are obtained with shadowing and the beam energy loss effect the suppression is the numerical results in ^{12}C is around 3 – 4%, and it increases with mass number and becomes around 8 – 9% in ^{184}W . The present theoretical results are also compared with E772 [37] experimental data.

In view of the E906 SeaQuest experiment being done at Fermi Lab, we have presented the results in Fig. 9, for $\frac{(\frac{d\sigma}{dx_t})_{p-A}}{(\frac{d\sigma}{dx_t})_{p-^2D}}$ vs x_t , ($A=^{12}\text{C}, ^{40}\text{Ca}, ^{56}\text{Fe}$ and ^{184}W), at $\sqrt{s_N}=15\text{GeV}$ corresponding to the energy of the incident proton $E=120\text{GeV}$. We find that the effect of spectral function to be around 7 – 8% in ^{12}C which increases with mass number and becomes around 8 – 9% in ^{184}W . When mesonic effects are included the rise in the DY ratio is around 11 – 12% in ^{12}C which increases with mass number and becomes around 13 – 14% in ^{184}W . When shadowing and energy loss effects are further added, then there is large reduction which is mainly due to loss of beam energy at low \sqrt{s} , which increases considerably with the increase in mass number of target nuclei. For example, for $\alpha=1$ in Eq. (27) the results are reduced by 22 – 24% in ^{12}C , 30 – 32% in ^{40}Ca and ^{56}Fe , and 42 – 44% in ^{184}W . To see the dependence of the different approaches of energy loss effect on the DY ratio, we have also obtained the results using $\gamma = 0.2$ in Eq. (28), and find that for low mass nuclei there is difference in the results of about 8-10% in ^{12}C , which becomes negligible with the increase in mass number of nuclear target.

In E866 experiment [30, 38], the results were obtained for $\frac{d\sigma}{dx_F}$ vs x_F , where $x_F = x_b - x_t$ and $\frac{d\sigma}{dM}$ vs M , with $M = \sqrt{x_b x_t s_N}$. Using Eqs.31 and 34, we have obtained the results respectively for $\frac{d\sigma}{dx_F}$ vs x_F and $\frac{d\sigma}{dM}$ vs M and shown these results in Fig.10. For $\frac{d\sigma}{dx_F}$ vs x_F , we have integrated over x_b between the limits $0.21 \leq x_b \leq 0.95$ and followed the kinematical cuts of $4.0 < M < 8.4\text{ GeV}$ used in the analysis of E866 [30, 38] experiment. In the case of $\frac{d\sigma}{dM}$ vs M , we have integrated over x_b between the limits $0.21 \leq x_b \leq 0.95$ and put the kinematical constraint $0.13 \leq x_F \leq 0.93$ as used in E866 [30, 38] experiment. These results are shown for the DY ratio for $\frac{(\frac{d\sigma}{dx_F})^i}{(\frac{d\sigma}{dx_F})^{Be}}$ vs

x_F (Left panel) and $\frac{(\frac{d\sigma}{dM})^i}{(\frac{d\sigma}{dM})^{Be}}$ vs M (Right panel), where i stands for iron (top panel) and tungsten (bottom panel) nuclei. These results are obtained with spectral function, including mesonic effect, and using our full model with energy loss effect. For the energy loss, we have used Eq.(27) with $\alpha = 1$. We observe that the effect of spectral function ($\sim 1\%$) and meson cloud contributions ($\sim 2\%$) are small. When shadowing and energy loss effects are included there is a significant reduction in DY yield which is around 4 – 5% in $\frac{Fe}{Be}$ and the reduction increases to 8 – 10% in $\frac{W}{Be}$. We find a good agreement with the experimental results for the various DY ratios available from E866 [30, 38] experiment.

In Fig. 11, we present the results of DY ratio for $\frac{(\frac{d^2\sigma}{dx_b dM})^{Fe}}{(\frac{d^2\sigma}{dx_b dM})^{Be}}$ vs x_b for different values of $M(=\sqrt{x_b x_t s_N})$, between the kinematic limits $0.13 \leq x_F \leq 0.93$ and $0.21 \leq x_b \leq 0.95$ as used in E866 experiment [49, 50]. The results of this ratio for $\frac{(\frac{d^2\sigma}{dx_b dM})^W}{(\frac{d^2\sigma}{dx_b dM})^{Be}}$ are shown in Fig. 12. The results are presented to observe the effect for spectral function, meson cloud contributions, and with shadowing effect and energy loss effect on the DY production.

IV. SUMMARY AND CONCLUSION

We have studied nuclear medium effects in DY process using quark parton distribution functions and nucleon structure functions for a bound nucleon. We have used a microscopic nuclear model which takes into account the effect of Fermi motion, nuclear binding and nucleon correlations through a relativistic spectral function of bound nucleon. The contributions of π and ρ mesons are also included. Furthermore, shadowing corrections are taken into account. We have also included the beam energy loss effect due to initial state interactions of protons with nuclear constituents before they suffer hard collisions to produce lepton pair. We find a reduction in the DY yield due to

nuclear structure effects and an enhancement due to mesonic contribution. The effect of shadowing is to reduce the DY yield in the region of very low x_t ($x_t < 0.15$). Both the reduction as well as the enhancement in the case of DY yields are found to be of similar magnitude as in the case of DIS of charged leptons. In the case of DY yields there is a further reduction due to beam energy loss effect in the nuclear medium which has been treated phenomenologically using a parameter describing the beam energy loss. The numerical results are compared with the experimental results from E772 [37] and E866 [30, 38] experiments. A reasonable agreement with the experimental results presently available for ^{12}C , ^{40}Ca , ^{56}Fe , and ^{184}W has been found. We have also presented in this paper, results for $\frac{d^2\sigma}{dx_b dx_t}$ vs x_b for various values of $M(=\sqrt{x_b x_t s_N})$ and the results for $\frac{d\sigma}{dx_t}$ vs x_t relevant to the forthcoming E906 SeaQuest [39] experiment at Fermi Lab. Our results show that the model for describing the nuclear medium effects in the DIS of charged leptons and neutrino and antineutrino with nuclear targets is able to explain the experimental results in the case of DY yield in the region $0.1 < x_t < 0.35$. High statistics, high precision data from E906 SeaQuest [39] experiment on $\frac{d^2\sigma}{dx_b dx_t}$ in various regions of x_b and x_t will provide important information about the modification of quark PDFs and nucleon structure function in the nuclear medium.

V. ACKNOWLEDGMENTS

M. S. A. is thankful to Department of Science and Technology(DST), Government of India for providing financial assistance under Grant No. SR/S2/HEP-18/2012. I.R.S. thanks FIS2014-59386-P Spanish project for financial support and Juan de la Cierva-incorporacion contract from Spanish MINECO.

-
- [1] S. D. Drell and Tung-Mow Yan, Phys. Rev. Lett. **25**, 316 (1970), Erratum-ibid. **25**, 902 (1970).
 - [2] Deep Inelastic Scattering, Robin Devenish and Amanda Cooper-Sarkar, Oxford University Press, New York 2004.
 - [3] I. R. Kenyon, Rep. Prog. Phys. **45**, 1261 (1982).
 - [4] D. F. Geesaman, K. Saito and A. W. Thomas, Ann. Rev. Nucl. Part. Sci. **45**, 337 (1995).
 - [5] K. J. Eskola, H. Paukkunen, C. A. Salgado, JHEP **0904** (2009), 065; K. J. Eskola, V. J. Kolhinen, H. Paukkunen and C. A. Salgado, JHEP **0705**, 002 (2007), S. Kumano, Phys. Rev. D **43**, 59 (1991); **43**, 3067 (1991), M. Hirai, S. Kumano and T. -H. Nagai, Phys. Rev. C **76**, 065207 (2007), M. Hirai, S. Kumano and T. -H. Nagai, Phys. Rev. C **70**, 044905 (2004).
 - [6] I. Schienbein, J.Y. Yu, C. Keppel, J.G. Morfin, F. Olness and J.F. Owens, Phys. Rev. D **77**, 054013 (2008), I. Schienbein, J.Y. Yu, K. Kovarik, C. Keppel, J.G. Morfin, F. Olness, J.F. Owens, Phys. Rev. D **80** 094004 (2009).
 - [7] R. P. Bickerstaff, M. C. Birse, and G. A. Miller, Phys. Rev. Lett. **53**, 2532 (1984).
 - [8] S. A. Kulagin and R. Petti, Phys. Rev. C **90**, 045204 (2014).
 - [9] S. A. Kulagin and R. Petti, Nucl. Phys. A **765**, 126 (2006); ibid Phys. Rev. D **76**, 094023 (2007).
 - [10] C. H. Llewellyn Smith, Phys. Lett. B **128**, 107 (1983).
 - [11] C. E. Carlson and T. J. Havens Phys. Rev. Lett. **51**, 261 (1983).
 - [12] F. E. Close, R. G. Roberts and G. G. Ross, Phys. Lett. B **129**, 346 (1983).
 - [13] M. Ericson and A. W. Thomas, Phys. Lett. B **148**, 191 (1984).
 - [14] E. L. Berger and F. Coester, Phys. Rev. D **32**, 1071 (1985).
 - [15] H. Jung and G. A. Miller, Phys. Rev. C **41**, 659 (1990).
 - [16] F. E. Close, R. L. Jaffe, R. G. Roberts and G. G. Ross, Phys. Rev. D **31**, 1004 (1985).
 - [17] G. E. Brown, M. Buballa, Z. B. Li and J. Wambach, Nucl. Phys. A **593**, 295 (1995).
 - [18] E. L. Berger, F. Coester and R. B. Wiringa, Phys. Rev. D **29**, 398 (1984).
 - [19] R. L. Jaffe and X. -D. Ji, Phys. Rev. Lett. **67**, 552 (1991).
 - [20] A. E. L. Dieperink and C. L. Korpa, Phys. Rev. C **55**, 2665 (1997).
 - [21] C. L. Korpa and A. E. L. Dieperink, Phys. Rev. C **87**, 014616 (2013).
 - [22] F. Eichstaedt, S. Leupold and U. Mosel, Phys. Rev. D **81**, 034002 (2010).
 - [23] E. Marco and E. Oset, Nucl. Phys. A **645**, 303 (1999).
 - [24] C.-G. Duan, L.-H. Song, S.-H. Wang, G.-L. Li Eur. Phys. J. C **39** (2005) 179.
 - [25] M. B. Johnson et al., Phys. Rev. C **65**, (2002) 025203.
 - [26] M. B. Johnson *et al.* [FNAL E772 Collaboration], Phys. Rev. Lett. **86**, 4483 (2001).
 - [27] F. Arleo, Phys. Lett. B **532**, 231 (2002)
 - [28] G. T. Garvey and J. C. Peng, Phys. Rev. Lett. **90** (2003) 092302.
 - [29] S. J. Brodsky and P. Hoyer, Phys. Lett. B **298**, 165 (1993).
 - [30] M. A. Vasiliev et al., Phys. Rev. Lett. **83**, 2304 (1999).
 - [31] E. Marco, E. Oset, and P. Fernandez de Cordoba, Nucl. Phys. A **611**, 484 (1996).
 - [32] M. Sajjad Athar, I. Ruiz Simo and M. J. Vicente Vacas, Nucl. Phys. A **857**, 29 (2011).
 - [33] H. Haider, I. Ruiz Simo, M. Sajjad Athar and M. J. Vicente Vacas, Phys. Rev. C **84**, 054610 (2011).

- [34] H. Haider, I. Ruiz Simo and M. Sajjad Athar, Phys. Rev. C **85**, 055201 (2012).
- [35] H. Haider, F. Zaidi, M. Sajjad Athar, S. K. Singh and I. Ruiz Simo, Nucl. Phys. A **943**, 58 (2015).
- [36] H. Haider, F. Zaidi, M. S. Athar, S. K. Singh and I. R. Simo, Nucl. Phys. A (in Press).
- [37] D. M. Alde et al., Phys. Rev. Lett. **64**, 2479 (1990).
- [38] E. A. Hawker et al. (FNAL E866/NuSea), Phys. Rev. Lett. **80**, 3715 (1998).
- [39] P. E. Reimer (Fermilab SeaQuest Collaboration), J. Phys.: Conf. Ser. **295**, 012011 (2011).
- [40] P. Fernandez de Cordoba and E. Oset, Phys. Rev. C **46**, 1697 (1992).
- [41] L. L. Frankfurt and M. Strikman Phys. Lett.B 183 1987 254.
- [42] Pavel M. Nadolsky et al., Phys. Rev. D **78**, 013004 (2008); <http://hep.pa.msu.edu/cteq/public>
- [43] M. Gluck, E. Reya and A. Vogt, Z. Phys. C **53**, 651 (1992).
- [44] C. G. Duan, N. Liu and Z. Y. Yan, Eur. Phys. J. C **50**, 585 (2007).
- [45] C. G. Duan, N. Liu and G. L. Li, Phys. Rev. C **79**, 048201 (2009).
- [46] S. Gavin and J. Milana, Phys. Rev. Lett. **68**, 1834 (1992).
- [47] A. Accardi, F. Arleo, W. K. Brooks, D. D'Enterria and V. Muccifora, Riv. Nuovo Cim. **32**, 439 (2010).
- [48] M. Lacombe *et al.*, Phys. Lett. B **101**, 139 (1981).
- [49] <http://durpdg.dur.ac.uk/review/dy/>
- [50] <http://p25ext.lanl.gov/e866/papers/papers.html>